University Library

MINERVA ACCESS

A gateway to Melbourne's research publications

Minerva Access is the Institutional Repository of The University of Melbourne

Author/s:
Shin, S;Kim, CJ;Goudeli, E;Faria, M;Cortez-Jugo, C;Caruso, F

Title:
Engineering Metal–Phenolic Network Materials through Compositional Tuning of Phenolic Molecules

Date:
2025

Citation:
Shin, S., Kim, C. J., Goudeli, E., Faria, M., Cortez-Jugo, C. & Caruso, F. (2025). Engineering Metal–Phenolic Network Materials through Compositional Tuning of Phenolic Molecules. Small, 21 (51), https://doi.org/10.1002/smll.202509224.

Persistent Link:
https://hdl.handle.net/11343/361491

Check for updates

WILEY-VCH

Engineering Metal–Phenolic Network Materials through Compositional Tuning of Phenolic Molecules

*Subin Shin, Chan-Jin Kim, Eirini Goudeli, Matthew Faria, Christina Cortez-Jugo, and Frank Caruso**

S. Shin, C.-J. Kim, E. Goudeli, C. Cortez-Jugo, F. Caruso
Department of Chemical Engineering, The University of Melbourne, Parkville, Victoria 3010, Australia
E-mail: fcaruso@unimelb.edu.au

C.-J. Kim
Department of Chemical Engineering, Gyeongsang National University, Jinju 52828, Republic of Korea

M. Faria
Department of Biomedical Engineering, The University of Melbourne, Parkville, Victoria 3010, Australia

Keywords: mechanical properties, oxidation-mediated assembly, particle engineering, polyphenols, supramolecular chemistry

Metal–phenolic coordination between polyphenols and metal ions is a well-established chemistry for preparing supramolecular assemblies. The selection of building blocks for assembly can influence the physicochemical properties of the assembled structures (e.g., morphology, permeability, and functionality). Herein, we demonstrate the compositional engineering of commercially available tannic acid (a commonly used polyphenol in assembly) to tailor the properties of metal–phenolic network (MPN) capsules. Through purification via preparative high-performance liquid chromatography, the composition of commercial tannic acid (cTA)—which consists of a mixture of phenolic compounds—was refined into "purified" tannic acid (pTA) that consists mainly of large molecular weight species. Assembling pTA with Fe^{II} ions, mediated by the oxidation of Fe^{II} to Fe^{III}, yielded MPN capsules with thicker (3×) films, increased stiffness (by ~70%) and reduced film permeability (~3×) compared with MPN

Author Manuscript

This is the author manuscript accepted for publication and has undergone full peer review but has not been through the copyediting, typesetting, pagination and proofreading process, which may lead to differences between this version and the Version of Record. Please cite this article as doi: 10.1002/smll.71461

This article is protected by copyright. All rights reserved.

capsules prepared with cTA and Fe^{II}. Molecular dynamics simulations suggest these property differences are due to the different interaction energies between TA and metal ions, which are influenced by the presence of small molecular weight phenolic species e.g. gallic acid in cTA. This study highlights a strategy to tailor the properties of MPN materials through tuning the interaction energies and reaction kinetics of phenolic building blocks.

1. Introduction

Supramolecular assembly of building blocks (e.g., polymers[1,2] and phenolic ligands[3–6]) can yield robust and tunable films, surface coatings and particles[7-11] for a range of applications. Metal–phenolic networks (MPNs) are a class of metal–organic supramolecular assemblies formed through the coordination of metal ions[12–14] with phenolic ligands, such as tannic acid (TA),[15,16] epigallocatechin gallate,[17,18] gallic acid (GA),[18,19] and quercetin,[20] which possess catechol or galloyl groups. MPN assembly has enabled the rapid and simple preparation of hydrogels,[21] particles,[22] capsules,[23] and thin films as surface coatings[24] or as self-standing films[25] for a range of applications.

The structural and functional diversity of phenolic building blocks, from synthetic to natural polyphenols, enable modulation of the physicochemical properties of MPN assemblies. For example, the use of catechol-functionalized poly(ethylene glycol) blocks with different architectures and molecular weights (M_w) generated MPN capsules with tailorable properties (e.g., thickness, permeability, and cell association).[26] In another study, subtle structural differences between flavonoids resulted in significantly different coating efficiencies and assembly mechanisms of MPNs, highlighting the fine sensitivity of MPN formation to subtle molecular structures.[27] Commercially available polyphenols, often derived from natural plant-based sources, have been used extensively in MPN studies,[28] with the type of phenolic compound used (e.g., TA versus GA) influencing film and particle properties.[18,29]

In addition to monoligand-based studies, where MPNs are assembled using a single type of phenolic ligand, crude phenolic ligand mixtures derived directly from plants have been exploited as MPN building blocks. A phenolic extract from green tea, mainly composed of epigallocatechin gallate and epicatechin gallate, was used to form multiligand MPN systems.[28] The multiligand system had different properties to analogous MPN systems obtained using a single type of phenolic ligand. Similarly, a crude extract from eucalyptus leaves, consisting of multicomponent phenolic building blocks, was used to form MPN thin

This article is protected by copyright. All rights reserved.

Author Manuscript

16136829, 0, Downloaded from https://onlinelibrary.wiley.com/doi/10.1002/smll.202509224 by The University Of Melbourne, Wiley Online Library on [26/11/2025]. See the Terms and Conditions (https://onlinelibrary.wiley.com/terms-and-conditions) on Wiley Online Library for rules of use; OA articles are governed by the applicable Creative Commons License

films.[30] These studies explored binding between multiple phenolic ligands and metal ions and demonstrated that phenolic ligands with multiple chelating sites selectively bind to metal ions. Collectively, these studies highlight the role of phenolic building block composition on the interactive forces and properties of the resulting films. Therefore, we hypothesized that engineering the composition of phenolic building blocks could be a useful strategy to tune the properties of MPNs.

TA is commonly used as a building block in MPN research owing to its multidentate structure (five catechol and five galloyl groups) and high availability. TA is often simplistically regarded as a single phenolic molecule or a monoligand with a molecular formula of $C_{76}H_{52}O_{46}$ in many MPN studies. However, commercial TA (cTA) comprises mixtures of TA and various low M_w phenolic compounds such as GA, *n*-galloyl glucose, and methyl gallate, with varying numbers of functional groups depending on the plant source.[31-33] The composition of cTA from different suppliers and batches can differ in the type and ratio of phenolic building blocks due to variations in plant origins, harvests, and extraction methods.[34,35] Batch-to-batch inconsistencies of cTA building blocks can affect MPN formation at the nanoscale, underscoring the need to consider purification of samples. In particular, the effect of small phenolic building blocks on the assembly of MPNs from cTA is unclear. Understanding the influence of phenolic building block molecular composition on MPN properties can inform the design of materials tailored for diverse applications. Therefore, this study aims to address how the compositional engineering of cTA, i.e., by refining cTA to obtain purified tannic acid (pTA), influences the physicochemical properties of MPN assemblies.

Herein, we study the effect of TA building block composition on MPN properties and compare the intermolecular interactions within the MPN assemblies experimentally and through molecular dynamics (MD) simulations. cTA, which consists of a broad range of phenolic compounds (170–1855 Da), was purified by preparative high-performance liquid chromatography (HPLC) to yield pTA, which is composed of a narrow range of high M_w phenolic compounds (1393–1855 Da). To prepare the MPN assemblies and enhance the observation of ligand-induced effects, an oxidation-mediated MPN assembly approach was used. This method is based on the oxidation of Fe^{II} (to Fe^{III}) over a relatively long time (12 h) in aqueous media followed by coordination with phenolic ligands.[36] The physicochemical properties of the MPN assemblies, such as thickness, stiffness, and permeability, were tuned

This article is protected by copyright. All rights reserved.

Author Manuscript

16136829, 0, Downloaded from https://onlinelibrary.wiley.com/doi/10.1002/smll.202509224 by The University Of Melbourne, Wiley Online Library on [26/11/2025]. See the Terms and Conditions (https://onlinelibrary.wiley.com/terms-and-conditions) on Wiley Online Library for rules of use; OA articles are governed by the applicable Creative Commons License

depending on the phenolic ligand composition (i.e., cTA and pTA) and assembly time. MD simulations revealed the structurally different states of the cTA-based and pTA-based MPNs. This study demonstrates that compositional engineering of the phenolic building block directly influences the physicochemical properties of MPN assemblies, which can consequently guide their application.

2. Results and Discussion

2.1. Compositional Tuning of TA Phenolic Building Blocks

The refinement of cTA to separate the large M_w species containing TA was performed using HPLC (**Scheme 1**a). HPLC was first performed under gradient mode to analyze the cTA batch with greater sensitivity. The chromatogram of cTA featured eight distinct peaks (**Figure 1**a, Table S1), which confirmed the presence of a mixture of macromolecular species in cTA. The dominant peak observed at 15.1 min was identified as the main TA peak because larger molecules have a longer residence time in the HPLC column than lower M_w molecules. To confirm the presence of small phenolic impurities, GA (a smaller phenolic molecule) was analyzed separately under the same elution conditions. The HPLC chromatogram of GA showed a peak at 5.5 min (Figure S1a). Therefore, the peaks with short residence times in the cTA spectrum were attributed to low M_w phenolic species, including GA.

To isolate TA, the isocratic mode was used for simplicity and to increase the purification efficiency. cTA was analyzed for 30 min in isocratic mode using a water/acetonitrile mixture at a ratio of 8:2 (Figure S2a). A broader spectrum (at 254 nm) was obtained compared with that obtained in gradient mode. However, the spectral profile was similar to the gradient mode HPLC spectrum. It is possible that the small peaks appearing under gradient mode may not be detected in isocratic mode due to its lower resolution. To collect the fraction containing TA, we optimized the sample collection time by setting a time window of 9.5–10.5 min (Figure S2c) in isocratic mode. The injection volume and cTA concentration were optimized to maximize the purification yield (Figure S2d). The collected fraction of pTA was freeze-dried and the homogeneity of the sample was confirmed by HPLC in gradient mode; the chromatogram displayed a single significant peak at 15.5 min (Figure 1b), corresponding to the high M_w molecules in cTA.

This article is protected by copyright. All rights reserved.

Author Manuscript

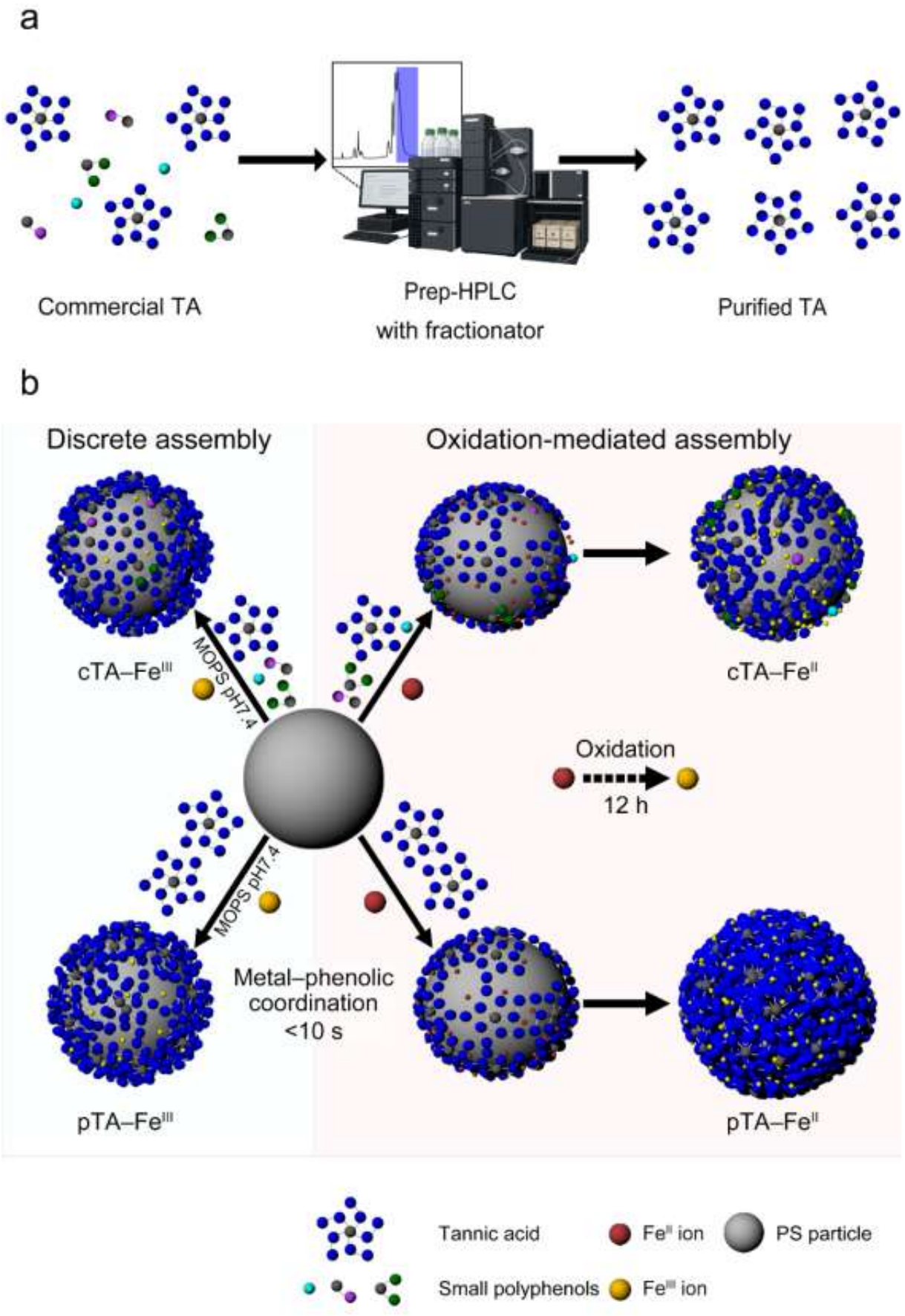
16136829, 0, Downloaded from https://onlinelibrary.wiley.com/doi/10.1002/smll.202509224 by The University Of Melbourne, Wiley Online Library on [26/11/2025]. See the Terms and Conditions (https://onlinelibrary.wiley.com/terms-and-conditions) on Wiley Online Library for rules of use; OA articles are governed by the applicable Creative Commons License

The mass profiles of cTA and pTA were analyzed by matrix-assisted laser desorption/ionization time-of-flight (MALDI-TOF) (Figure S3). The pTA spectrum showed a peak at *m*/*z* 1739, indicating the replacement of one of the hydrogen atoms (*m*/*z* 1.0) in the pTA molecule (*m*/*z* 1701.2) with a potassium atom (*m*/*z* 39.1) in the salt. Split peaks around the main peak were observed owing to the detachment and attachment of galloyl benzene groups (154.1 g mol^{-1}) to the pTA molecules (Figure S3). When compared with the spectrum of pTA, the MALDI-TOF spectrum of cTA showed a main peak at *m*/*z* 1431 and a general distribution at lower *m*/*z* values. This confirms that smaller phenolic species, in which one or more galloyl benzene groups are detached, are present and are more predominant in cTA than in pTA.

Author Manuscript

This article is protected by copyright. All rights reserved.

16136829, 0, Downloaded from https://onlinelibrary.wiley.com/doi/10.1002/smll.202509224 by The University Of Melbourne, Wiley Online Library on [26/11/2025]. See the Terms and Conditions (https://onlinelibrary.wiley.com/terms-and-conditions) on Wiley Online Library for rules of use; OA articles are governed by the applicable Creative Commons License



Scheme 1. (a) Schematic of the refinement of cTA into pTA using preparative HPLC (Prep-HPLC). (b) Schematic of discrete and oxidation-mediated MPN assembly using cTA or pTA.

This article is protected by copyright. All rights reserved.

Author Manuscript

16136829, 0, Downloaded from https://onlinelibrary.wiley.com/doi/10.1002/smll.202509224 by The University Of Melbourne, Wiley Online Library on [26/11/2025]. See the Terms and Conditions (https://onlinelibrary.wiley.com/terms-and-conditions) on Wiley Online Library for rules of use; OA articles are governed by the applicable Creative Commons License

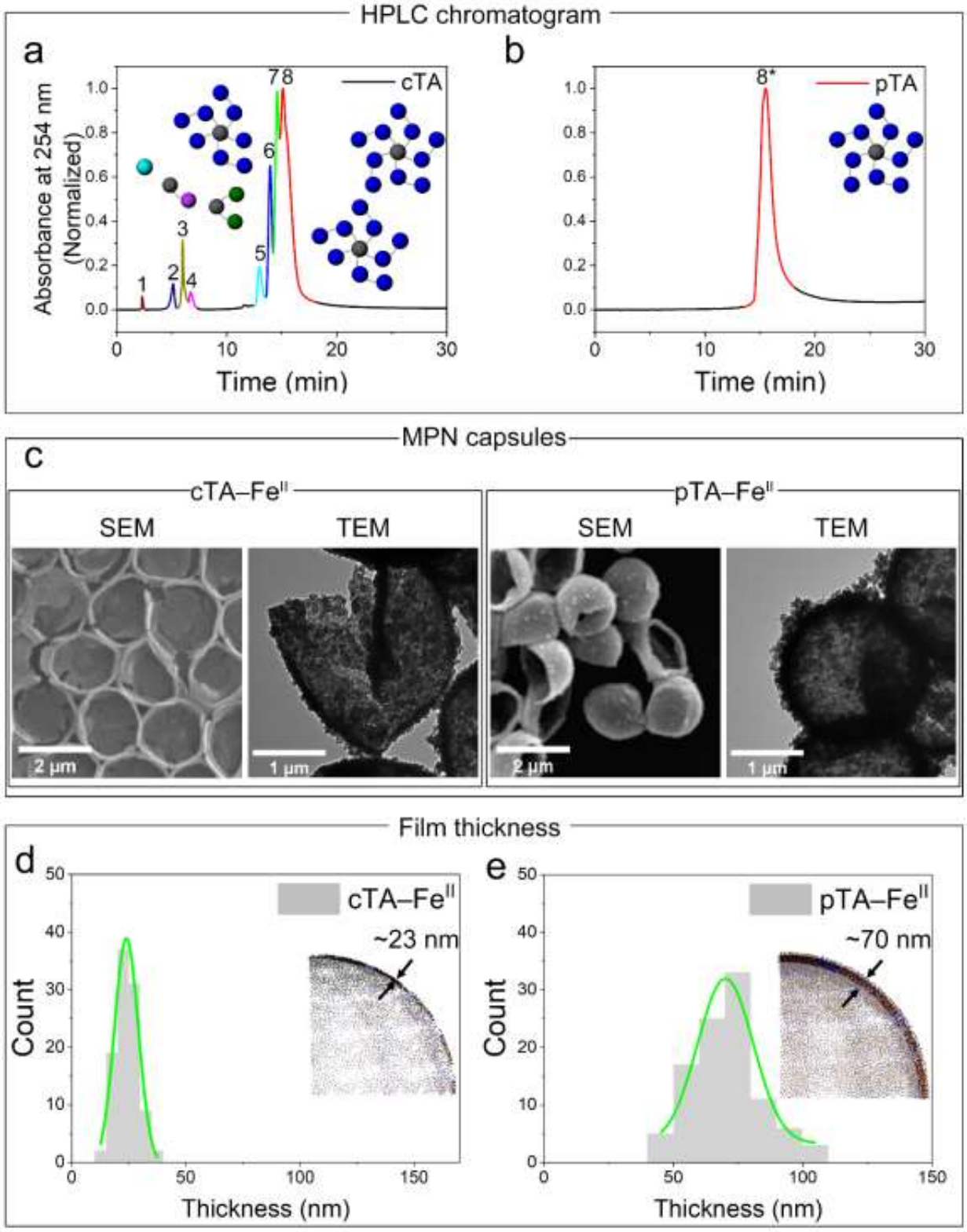


Figure 1. (a,b) HPLC chromatographs of cTA (a) and pTA (b). The colored peaks represent the different components in the HPLC samples; HPLC peak areas are summarized in Table S1. (c) SEM and TEM images (magnification 5000×) of MPN capsules prepared via OA using Fe^{II} and cTA or pTA. (d,e) Capsule thickness histograms and gaussian fit curves (in green color) of cTA–Fe^{II} capsules (d) and pTA–Fe^{II} capsules prepared via OA after 12 h synthesis. Histograms were obtained from thickness measurements of 100 capsules from TEM images.

This article is protected by copyright. All rights reserved.

Author Manuscript

16136829, 0, Downloaded from https://onlinelibrary.wiley.com/doi/10.1002/smll.202509224 by The University Of Melbourne, Wiley Online Library on [26/11/2025]. See the Terms and Conditions (https://onlinelibrary.wiley.com/terms-and-conditions) on Wiley Online Library for rules of use; OA articles are governed by the applicable Creative Commons License

2.2. MPN Capsule Assembly from pTA and cTA

We next examined the effect of phenolic composition (i.e., pTA and cTA) on metal–phenolic complexation and the physical properties of the resulting MPN assemblies. MPN capsules were first prepared by discrete assembly (DA), which is a common, simple, and rapid technique (within seconds) for forming MPNs on a template surface.[12] Briefly, polystyrene (PS) templates were dispersed in the phenolic (cTA or pTA) solution and mixed with the metal ion (Fe^{III}) solution by vortexing for 5 s. The pH of the resulting MPN solution was adjusted using (3-morpholinopropane-1-sulfonic acid) buffer at pH 8. Finally, the PS templates of the MPN-coated particles were removed by dissolution with tetrahydrofuran. The resulting MPN capsules prepared by DA—i.e., cTA–Fe^{III} and pTA–Fe^{III}—were analyzed by scanning electron microscopy (SEM), transmission electron microscopy (TEM), and atomic force microscopy (AFM) (Figure S4). There were no significant differences between cTA–Fe^{III} and pTA–Fe^{III} in terms of particle size, shape, or thickness, despite the different composition of phenolic compounds used in capsule preparation. This finding suggests that the multiple chelating sites present on large polyphenols (i.e., TA) play a more dominant role over the small phenolic ligands during MPN formation by DA, owing to the high reactivity and stability between Fe^{III} and TA[30] and to the different coordination modes of TA–Fe^{III} and, for example, GA–Fe^{III}, during film formation.[18]

MPN films can also be prepared via oxidation-mediated assembly (OA), which uses Fe^{II} that is slowly oxidized to Fe^{III} during network formation.[36] This method affords reversibility and self-correction of chemical interactions involved during MPN fabrication as the slower coordination reaction time enables gradual coordination between metal ions and phenolic ligands, allowing conformational changes and molecular rearrangement of the coordination to occur over time[37] These dynamic changes result in phenolic components that potentially exert a greater influence on MPN properties when compared with those involved in DA. The MPN capsules, prepared via OA, were obtained by mixing either cTA or pTA and an Fe^{II} solution with PS particles and stirring for 12 h (Scheme 1b). During MPN assembly, the reaction mixture was exposed to the atmosphere to allow oxidation of the MPN capsules in the presence of dissolved oxygen.[36,38] During assembly, the pH was not altered and PS templates were dissolved using the same protocol as that used for DA.

This article is protected by copyright. All rights reserved.

Author Manuscript

16136829, 0, Downloaded from https://onlinelibrary.wiley.com/doi/10.1002/smll.202509224 by The University Of Melbourne, Wiley Online Library on [26/11/2025]. See the Terms and Conditions (https://onlinelibrary.wiley.com/terms-and-conditions) on Wiley Online Library for rules of use; OA articles are governed by the applicable Creative Commons License

Consistent with our previous study, phenolic ligands and Fe^{II} mixtures resulted in slower (>12 h) MPN formation, which was evident from the slower color change of the solution from bright purple to a darker purple when compared with that observed for DA (dark purple color was instant).[38] The oxidation of Fe^{II} ions is the rate-determining step in OA, as Fe^{II} is much less reactive and less stable than Fe^{III} in terms of complexation with phenolic ligands (i.e., stability constants, log K_1, of Fe^{II} and Fe^{III} are ≈8 and ≈20, respectively). [39]

Using OA, the MPN capsules synthesized with cTA (i.e., cTA–Fe^{II}) differed significantly from those synthesized with pTA (i.e., pTA–Fe^{II}). SEM and TEM images show that the pTA–Fe^{II} capsules were thicker than the cTA–Fe^{II} capsules (Figure 1c–e). Electron microscopy of the air-dried samples showed collapsed cTA–Fe^{II} capsules, whereas pTA–Fe^{II} capsules remained spherical. The shell thickness of the two capsule types, as determined by the outer layer in TEM images,[40] differed significantly (i.e., 70 ± 13 nm for pTA–Fe^{II} capsules and 23 ± 5 nm for cTA–Fe^{II} capsules). This finding is in contrast to the capsules formed by DA, which showed no significant difference in shape or thickness between cTA–Fe^{III} and pTA–Fe^{III} capsules (Figure S4).

2.3. Effect of MPN Assembly Time on Capsule Properties

The most notable difference between OA and DA is the time needed to assemble MPNs. cTA–Fe and pTA–Fe capsules were synthesized at different time points to determine the effect of synthesis time on the thickness and shape of the MPN capsules.

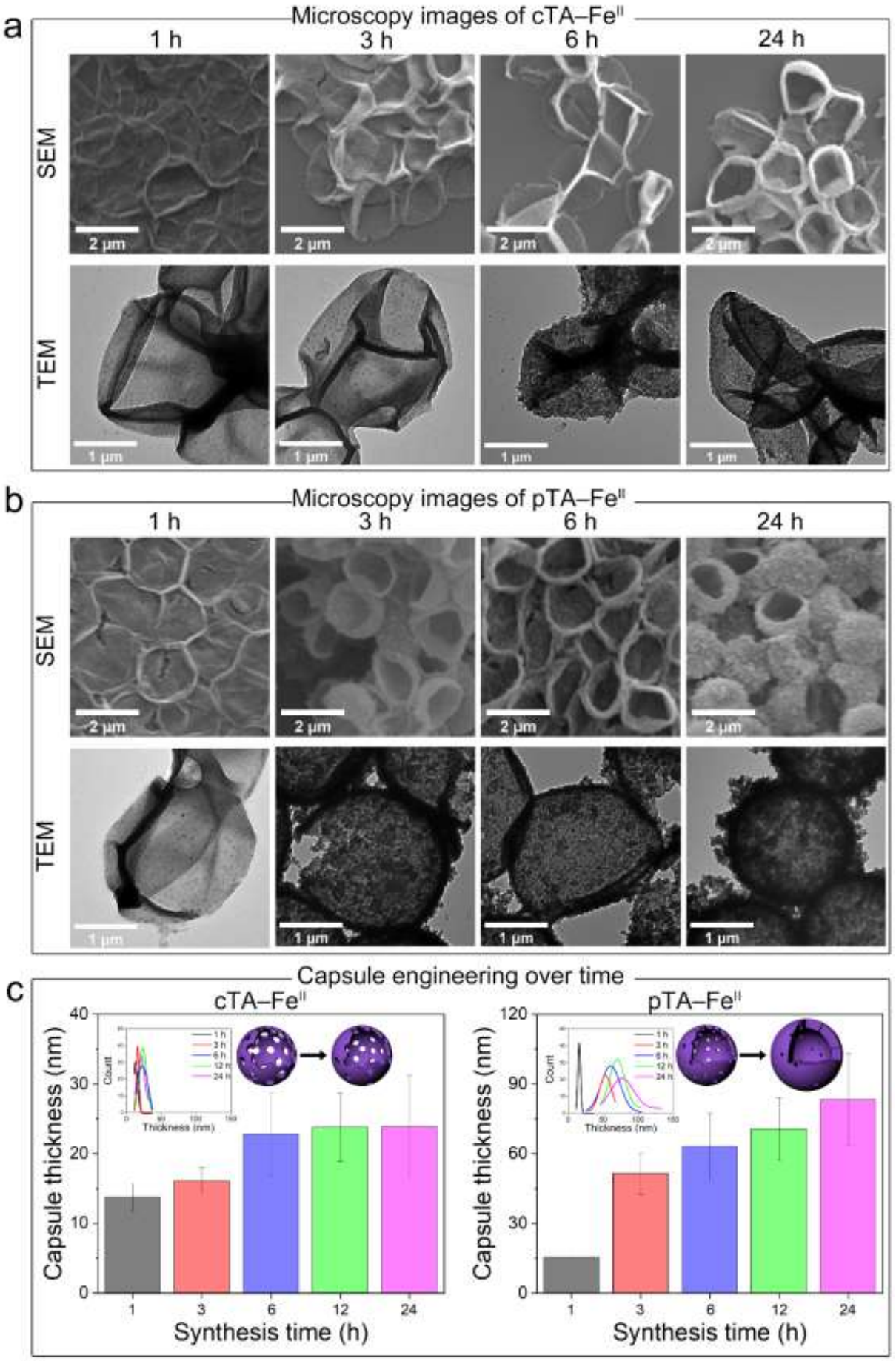
MPN synthesis on PS templates via DA was performed for 1–24 h and the capsule properties were analyzed. Given that complexation is rapid and complete within the synthesis time frames studied, the cTA–Fe^{III} and pTA–Fe^{III} MPNs capsules were comparable to each other in terms of morphology (Figure S4). In contrast, the MPN capsules obtained via OA displayed different shell thicknesses over time, which was also dependent on the phenolic molecule used (**Figure 2**a,b). The cTA–Fe^{II} capsules had shell thicknesses of ~20 nm at 6 h, which remained constant up to 24 h (Figure 2c). The thickness of pTA–Fe^{II} capsules increased progressively with time (up to 24 h studied) from 15 ± 2 nm to 83 ± 20 nm, as measured from TEM images, with the MPN capsule shell becoming darker and thicker over time. Furthermore, SEM images show that at 24 h, the pTA–Fe^{II} capsules remained intact after PS template removal (Figure 2b), as consistent with a thicker MPN coating. Additionally, the

This article is protected by copyright. All rights reserved.

Author Manuscript

16136829, 0, Downloaded from https://onlinelibrary.wiley.com/doi/10.1002/smll.202509224 by The University Of Melbourne, Wiley Online Library on [26/11/2025]. See the Terms and Conditions (https://onlinelibrary.wiley.com/terms-and-conditions) on Wiley Online Library for rules of use; OA articles are governed by the applicable Creative Commons License

capsules displayed fewer defects and rougher surfaces with prolonged synthesis times, indicating ongoing MPN formation.



This article is protected by copyright. All rights reserved.

Author Manuscript

16136829, 0, Downloaded from https://onlinelibrary.wiley.com/doi/10.1002/smll.202509224 by The University Of Melbourne, Wiley Online Library on [26/11/2025]. See the Terms and Conditions (https://onlinelibrary.wiley.com/terms-and-conditions) on Wiley Online Library for rules of use; OA articles are governed by the applicable Creative Commons License

Figure 2. SEM and TEM images (magnification 5000×) of (a) cTA–Fe^{II} and (b) pTA–Fe^{II} capsules prepared via OA using different reaction times. (c) Capsule thickness as a function of synthesis time. Thickness measurements were obtained from 100 capsules from TEM images. Insets show capsule thickness gaussian fit curves and schematic illustrations of increasing thickness of cTA–Fe^{II} and pTA–Fe^{II} capsules prepared by OA over time.

2.4. Mechanical Properties of MPN Capsules

The mechanical properties (i.e., permeability, stiffness, and stability) of the MPN capsules were also assessed to determine the influence of phenolic ligand composition. Capsule permeability, which is influenced by the density, thickness, and pore size of the MPNs,[5] was expected to vary between cTA–Fe^{II} and pTA–Fe^{II} capsules, owing to their different shell thicknesses. Confocal laser scanning microscopy was used to assess the permeability of the MPN capsules toward fluorescein isothiocyanate-labeled dextran (FITC-dextran) with different M_w. FITC-dextran can pass through the pores of MPN capsules if the pore sizes are large enough or if the density of the film is low.[26,41] Permeability was calculated as the percentage of capsules permeable to FITC-dextran. Capsules were considered impermeable if the fluorescence inside the capsule was less than 75% of the background signal. Because of the negligible shell thickness differences of the cTA–Fe^{III} and pTA–Fe^{III} capsules formed via DA, the capsules exhibited similar permeability across the range of FITC-dextran M_w used (Figure S5). In contrast, the pTA–Fe^{II} and cTA–Fe^{II} capsules formed via OA showed different degrees of permeability—pTA–Fe^{II} capsules were less permeable than cTA–Fe^{II} capsules across the FITC-dextran M_w range studied (**Figure 3**a). For instance, pTA–Fe^{II} capsules displayed lower permeability to 4 kDa FITC-dextran (~25%) than cTA–Fe^{II} capsules (~70%) (Figure 3a). The permeability difference was consistent across different thresholds of capsule permeability (i.e., 60%, 75%, and 90% of background fluorescence, Figure S6). The reduced permeability of the pTA–Fe^{II} capsules is likely due to their thicker shells compared to the cTA–Fe^{II} capsules, although an increase in network density may also play a role.

Previous studies have shown that capsule thickness influences the mechanical properties of MPN capsules.[28,40-42] Therefore, the stiffness of the pTA–Fe and cTA–Fe capsules was assessed using AFM under liquid phase to keep the capsules hydrated, thus resisting collapse and maintaining their spherical shape. A colloid-modified AFM tip was used to obtain force–distance correlation plots between the tip and the capsules (Figure 3b). Only a small difference (<3.4%) in stiffness was observed between cTA–Fe^{III} (337 ± 94 mN m^{-1}) and

This article is protected by copyright. All rights reserved.

Author Manuscript

16136829, 0, Downloaded from https://onlinelibrary.wiley.com/doi/10.1002/smll.202509224 by The University Of Melbourne, Wiley Online Library on [26/11/2025]. See the Terms and Conditions (https://onlinelibrary.wiley.com/terms-and-conditions) on Wiley Online Library for rules of use; OA articles are governed by the applicable Creative Commons License

pTA–Fe^{III} (349 ± 77 mN m^{-1}) capsules formed by DA (Figure S7). In contrast, the stiffness of cTA–Fe^{II} and pTA–Fe^{II} capsules differed, with pTA–Fe^{II} capsules displaying a stiffness of 765 ± 82 mN m^{-1}, which was 71% higher than the stiffness of cTA–Fe^{II} capsules (447 ± 68 mN m^{-1}) (Figure 3b,c). The difference in the stiffness between the cTA–Fe^{II} and pTA–Fe^{II} capsules is consistent with their differing thicknesses, confirming that thicker MPN capsules are more rigid, hence stiffer, than thinner capsules, although the possible influence of capsule density cannot be ruled out.

The stability of the capsules was also analyzed by incubating the capsules in 100 mM ethylenediaminetetraacetic acid (EDTA) at pH 8.0 for 24 h. EDTA solution is used to compete with metal coordination bonding between phenolic ligands and metal ions, which results in capsule disassembly. Flow cytometry was used to quantify the number of stable capsules remaining after each time point during incubation. As observed from Figure 3d, only 75% of cTA–Fe^{II} capsules remained intact after incubation in EDTA for 1 h compared with 95% of the pTA–Fe^{II} capsules after the same incubation time. Even at 24 h, 85% of the pTA–Fe^{II} capsules remained intact, whereas only 57% of cTA–Fe^{II} capsules remained stable.

Our findings show that the assembly method influences the physicochemical properties of MPN capsules, and this depends on the composition of phenolic building blocks, as demonstrated using cTA and pTA.

This article is protected by copyright. All rights reserved.

Author Manuscript

16136829, 0, Downloaded from https://onlinelibrary.wiley.com/doi/10.1002/smll.202509224 by The University Of Melbourne, Wiley Online Library on [26/11/2025]. See the Terms and Conditions (https://onlinelibrary.wiley.com/terms-and-conditions) on Wiley Online Library for rules of use; OA articles are governed by the applicable Creative Commons License

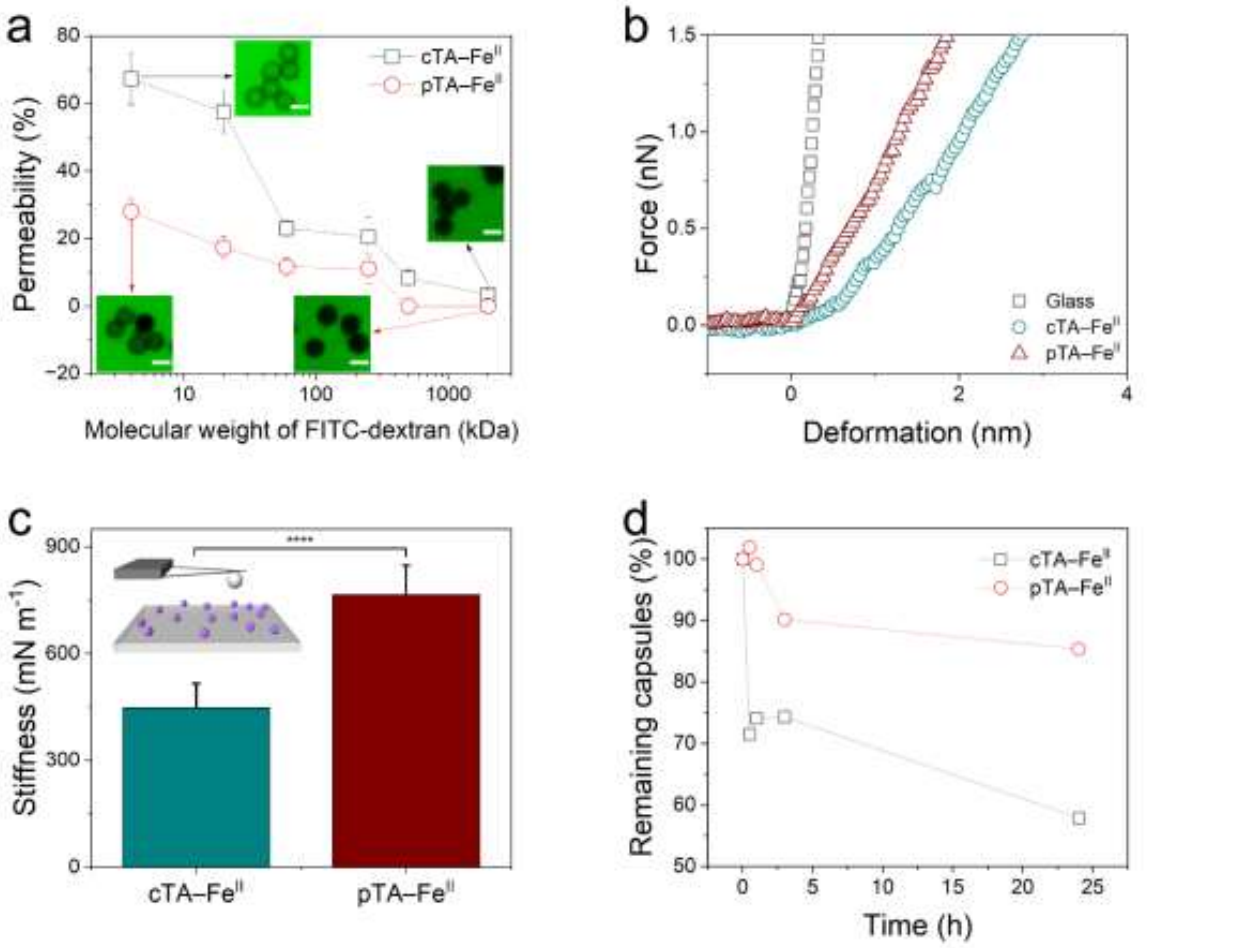


Figure 3. (a) Proportion of cTA–Fe^{II} and pTA–Fe^{II} capsules permeable to FITC-dextran with different M_w ranging between 4 and 2000 kDa. Data represent the proportion of permeable capsules (among 100 capsules) in confocal laser scanning microscopy images acquired with a 100× oil-immersion objective. Each sample was analyzed by measuring 100 capsules, and repeated three times to calculate the standard deviation. The insets show the corresponding confocal laser scanning microscopy images of the capsules permeable to FITC-dextran; scale bars = 2 μm. Capsules were synthesized via OA over 24 h. (b) Representative force–deformation curves of cTA–Fe^{II}, pTA–Fe^{II}, and glass substrate. (c) Representative stiffness of cTA–Fe^{II} and pTA–Fe^{II} capsules measured using liquid phase AFM. Stiffness is calculated from force–deformation curves from 15 capsules. Statistical significance was determined by an unpaired *t*-test and is reported as ****$p < 0.0001$. (d) Percentage of (stable) MPN capsules remaining after their incubation in 100 mM EDTA solution (pH 8), as assessed by flow cytometry.

2.5. Influence of GA on MPN Capsule Composition and Properties

To further investigate the influence of low M_w species in TA on MPN capsule properties, capsules were prepared via OA using pTA/GA mixtures with different molar ratios (i.e.,

Author Manuscript

This article is protected by copyright. All rights reserved.

16136829, 0, Downloaded from https://onlinelibrary.wiley.com/doi/10.1002/smll.202509224 by The University Of Melbourne, Wiley Online Library on [26/11/2025]. See the Terms and Conditions (https://onlinelibrary.wiley.com/terms-and-conditions) on Wiley Online Library for rules of use; OA articles are governed by the applicable Creative Commons License

100/0, 75/25, 50/50, 25/75, and 0/100, pTA/GA mol%). Although other low M_w species are present in cTA, GA was selected as a representative small molecule in our study because it shares the same galloyl functional group as TA and is approximately one-tenth of the M_w of TA, giving a clear distinction of M_w difference. GA also appears to be the most prominent low M_w impurity present in the stock of cTA used in this study (Table S1). The composition of GA in the resulting capsules was determined by disassembly of the capsules in strong acid (i.e., 2 M hydrochloric acid), followed by HPLC analysis. The MPN capsules prepared exclusively from pTA showed a predominant TA peak (Figure S8a), as consistent with earlier pTA analysis (Figure 1b). Minor peaks (which were not previously observed in Figure 1b) were also observed, likely owing to the harsh acidic conditions used to disassemble the capsules. Nevertheless, capsules prepared with GA-rich pTA mixtures showed a distinct increase in GA peak intensity, indicating that GA was incorporated into the capsule structure (Figure S8b–f). The higher number of chelating sites on TA leads to its preferential coordination (over lower M_w phenolic species) with metal ions but as the proportion of GA increases, GA also contributes to MPN formation (**Figure 4**a). Quantification of the pTA-to-GA weight ratio in the MPN capsule reveals that pTA remains the major phenolic component, particularly as its proportion in the feed solution increases (Figure 4b). However, the incorporation of GA into the capsules alongside TA suggests that low M_w phenolic ligands, such as GA, can participate in MPN formation and potentially influence the final MPN structure and capsule properties. To demonstrate this, we investigated the influence of GA on capsule permeability using 4 kDa FITC-dextran as the probe. As the proportion of GA increased in the phenolic mixture, capsule permeability likewise increased from ~24% for pTA-only capsules to ~76% for GA-only capsules (Figure 4c). The addition of GA to TA leads to an increase in capsule shell permeability, which is consistent with the higher permeability of cTA-based MPN capsules compared with pTA-based capsules (Figure 3a).

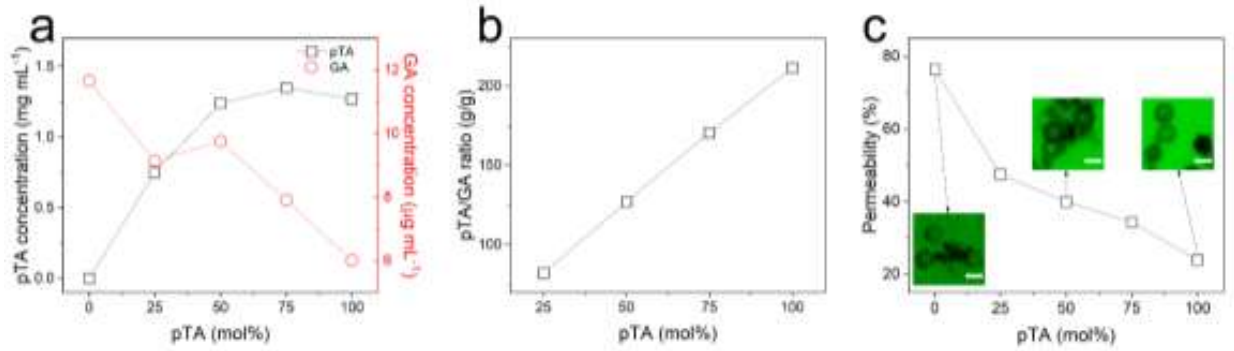


Figure 4. (a) Concentrations of pTA and GA within MPN capsules formed from phenolic mixtures with varying pTA and GA proportions, as determined by HPLC analysis after

This article is protected by copyright. All rights reserved.

Author Manuscript

16136829, 0, Downloaded from https://onlinelibrary.wiley.com/doi/10.1002/smll.202509224 by The University Of Melbourne, Wiley Online Library on [26/11/2025]. See the Terms and Conditions (https://onlinelibrary.wiley.com/terms-and-conditions) on Wiley Online Library for rules of use; OA articles are governed by the applicable Creative Commons License

capsule disassembly. (b) Mass ratio of pTA to GA from the disassembled capsules plotted against pTA proportion in the phenolic mixture feed. (c) Percentage of pTA/GA–Fe^{II} capsules permeable to 4 kDa FITC-dextran. Permeability at increasing pTA proportion is shown. Data represent permeable capsule proportion among 50 capsules in confocal laser scanning microscopy images acquired with a 100× oil-immersion objective. The insets show the corresponding confocal laser scanning microscopy images of the capsules permeable to FITC-dextran; scale bars = 2 μm.

Our findings highlight the potential influence of low M_w phenolic ligands on MPN formation. They indicate that small phenolic ligands in a heterogenous mixture, such as cTA, may compete with interactions occurring between large polyphenols and metal ions, resulting in different material properties (e.g., permeability). However, this is only observable when OA is used, as the composition and properties of cTA–Fe^{III} and pTA–Fe^{III} formed by DA are comparable. We hypothesize that the slower kinetics of interaction between phenolic ligands and metal ions occurring during OA, limited by the oxidation of Fe^{II} to Fe^{III}, allows for diverse species of phenolic ligands in the mixture to interact and compete with the metal ions.

2.6. MD Simulation of MPNs Formed with pTA

To confirm our hypothesis that different interactions of phenolic ligands and metal ions in a mixture can influence film properties, MD simulations of MPN formation from cTA versus pTA were performed. In the MD simulations, the cTA component is simplified such that cTA consists only of TA and GA. The amount of TA and GA in the cTA batch was calculated from HPLC using pTA and GA standards (Figure S1). Different ratios of either Fe^{II} or Fe^{III} ions were added to cTA and pTA in the simulations to evaluate the interaction kinetics between the phenolic ligands and metal ions, simulating OA (with Fe^{II}) and DA (with Fe^{III}).

We first performed simulation studies to elucidate how the phenolic composition (pTA versus cTA) influences the porosity, and hence permeability, of MPNs. The deposition of phenolic ligands and Fe ions dispersed in water onto a PS substrate was simulated until film growth reached a steady state. For Fe^{II} and cTA (TA and GA mixture in the simulation), a highly porous film was formed with a nonhomogeneous network density (**Figure 5**a). MPNs formed with Fe^{II} and pTA (TA only in the simulation) resulted in a less porous, homogeneous film on the substrate. The simulation results are consistent with the permeability data and suggest that porosity contributes to the permeability of the cTA capsules. Examination of the interactions

This article is protected by copyright. All rights reserved.

Author Manuscript

16136829, 0, Downloaded from https://onlinelibrary.wiley.com/doi/10.1002/smll.202509224 by The University Of Melbourne, Wiley Online Library on [26/11/2025]. See the Terms and Conditions (https://onlinelibrary.wiley.com/terms-and-conditions) on Wiley Online Library for rules of use; OA articles are governed by the applicable Creative Commons License

within the cTA-based MPN (Figure 5a insets), particularly the interaction of GA with Fe^{II} ions, indicates that GA hinders the expansion of the network and acts as a terminal site—this is reflected by the formation of large pores in the network. Hence, cTA–Fe^{II} MPNs do not grow continuously. In the absence of interfering GA (i.e., in pTA), TA with multiple metal chelating sites can extend the MPN network. Consequently, pTA–Fe^{II} shows a denser and less porous network than the cTA–Fe^{II} network, as illustrated in **Scheme 2**.

The effect of GA on the expansion of the MPN network was also determined by calculating the potential of mean force, which gives an indication of the interaction strength between TA/Fe at the edge of a growing MPN film and a neighboring phenolic ligand (i.e., GA and TA) as a function of distance. Figure 5b (for Fe^{II}) and Figure S9b (for Fe^{III}) show that the interaction energy minimum state of TA/Fe–TA is lower than that of TA/Fe–GA, suggesting that the interaction of TA with Fe is more competitive and thermodynamically more favorable than the interaction between Fe ions and GA. When Fe^{III} ions are introduced to fabricate MPNs, metal coordination with TA is rapid (within seconds) and irreversible. In DA, TA/Fe^{III}–TA interaction is more dominant than TA/Fe^{III}–GA interaction (Figure S9b), hence TA can undergo rapid and nonreversible metal coordination with Fe^{III} ions, regardless of the presence of small phenolic ligands in the batch, resulting in similar MPN properties between cTA–Fe^{III} and pTA–Fe^{III}, as observed experimentally. In OA, the smaller interaction energy gap between TA/Fe^{II}–GA and TA/Fe^{II}–TA (20.94 kcal mol^{-1}) than the interaction energy gap between TA/Fe^{III}–GA and TA/Fe^{III}–TA (26.32 kcal mol^{-1}) indicates a more favorable interaction between small phenolic ligands and Fe^{II} than with Fe^{III}. Therefore, both TA and small phenolic ligands can interact with metal ions to form MPNs in cTA–Fe^{II}. Accordingly, distinct differences are observed in capsule thickness, permeability and mechanical properties, when single phenolic building blocks (e.g., pTA) are introduced in OA.

The distance between metal molecules was analyzed through simulation to model the density of the MPNs composed of pTA (TA_{21} in the simulation) or cTA ($TA_{20}GA_9$ mixture in the simulation) (Figure 5c). Assuming that all phenolic ligands in cTA interact with metal ions, the distance between metal ions in cTA–Fe^{II} would be expected to be shorter than that in pTA–Fe^{II}, because the distance between metals would be proportional to phenolic ligand size and cTA contains smaller phenolics. However, from the simulation, the radial distribution function between Fe^{II} ions (Figure 5c) reveals a slightly shorter average distance for the first Fe^{II}–Fe^{II} neighbors in pTA–Fe^{II} than in cTA–Fe^{II}. Based on the distance between metal ions,

Author Manuscript

This article is protected by copyright. All rights reserved.

16136829, 0, Downloaded from https://onlinelibrary.wiley.com/doi/10.1002/smll.202509224 by The University Of Melbourne, Wiley Online Library on [26/11/2025]. See the Terms and Conditions (https://onlinelibrary.wiley.com/terms-and-conditions) on Wiley Online Library for rules of use; OA articles are governed by the applicable Creative Commons License

it can be inferred that pTA–Fe^{II} is a denser, intra-network system than cTA–Fe^{II}, as suggested by the experimental permeability data. To determine whether other factors influence Fe–Fe distance, and hence MPN density, TA–Fe distances were also analyzed; no differences were observed in the distances between TA and Fe^{II} within cTA–Fe^{II} and pTA–Fe^{II} networks (Figure S10a).

To calculate the density of the MPNs more directly, we simulated the interaction of TA and increasing amount of GA (denoted as $TA_{20}GA_4$, $TA_{20}GA_6$, and $TA_{20}GA_9$) with metal ions, keeping the same number of molecules in a given space consistent. In simulating the interaction, the density of the total molecules is calculated until the density data is saturated (Figure 5d, Figure S9d). The results in Figure 5e revealed that regardless of the TA/GA ratio, the Fe^{III}-based MPNs showed comparable densities. In contrast, the density of the MPNs prepared with Fe^{II} decreased as the relative proportion of GA increased. Accordingly, MPNs prepared from pTA are denser than MPNs prepared from an unrefined mixture of phenolic ligands (cTA) and MPN properties can be controlled by composition tuning of the phenolic molecules (e.g., using pure polyphenols rather than a mixture of different types of phenolic ligands).

Author Manuscript

This article is protected by copyright. All rights reserved.

16136829, 0, Downloaded from https://onlinelibrary.wiley.com/doi/10.1002/smll.202509224 by The University Of Melbourne, Wiley Online Library on [26/11/2025]. See the Terms and Conditions (https://onlinelibrary.wiley.com/terms-and-conditions) on Wiley Online Library for rules of use; OA articles are governed by the applicable Creative Commons License

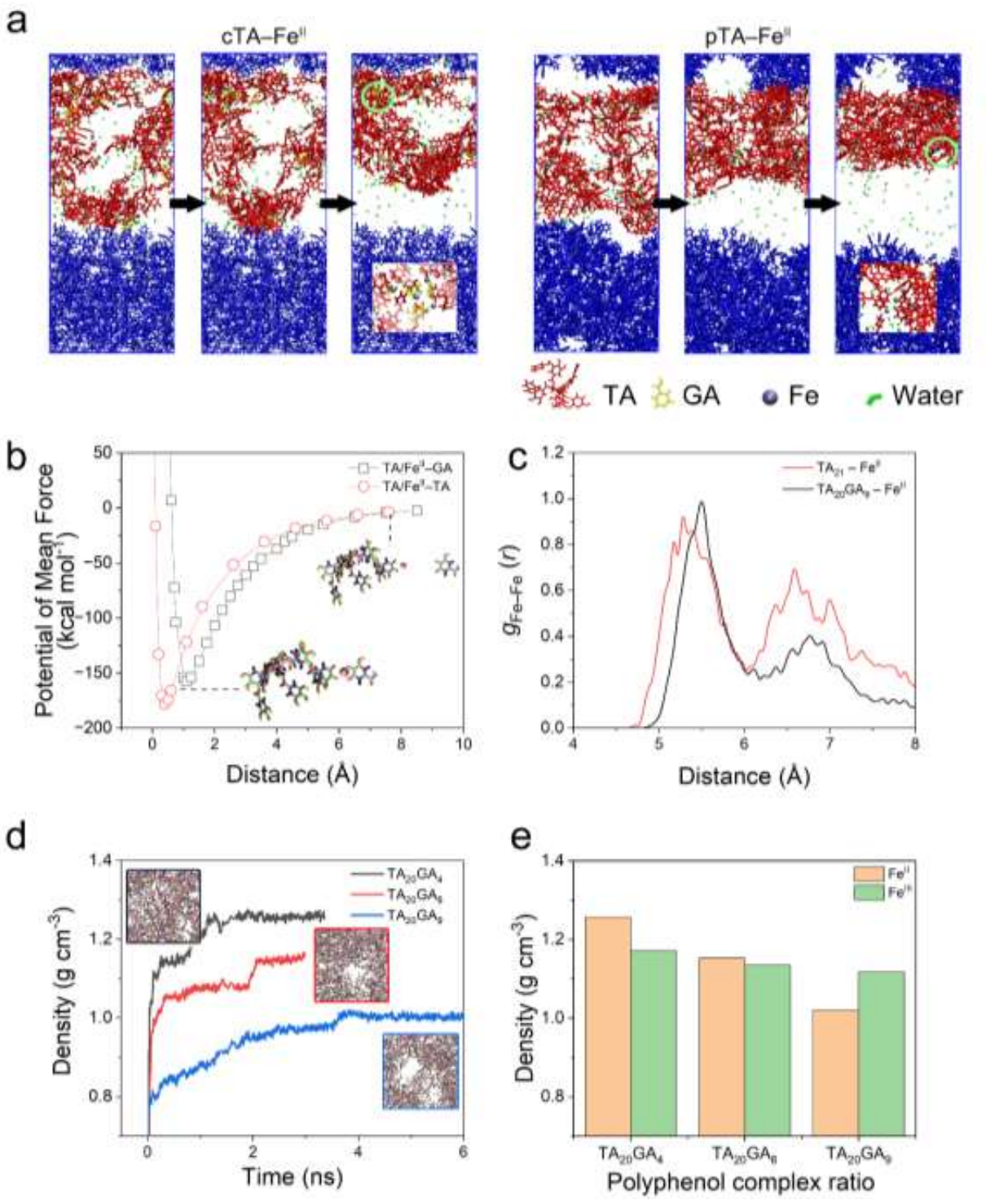


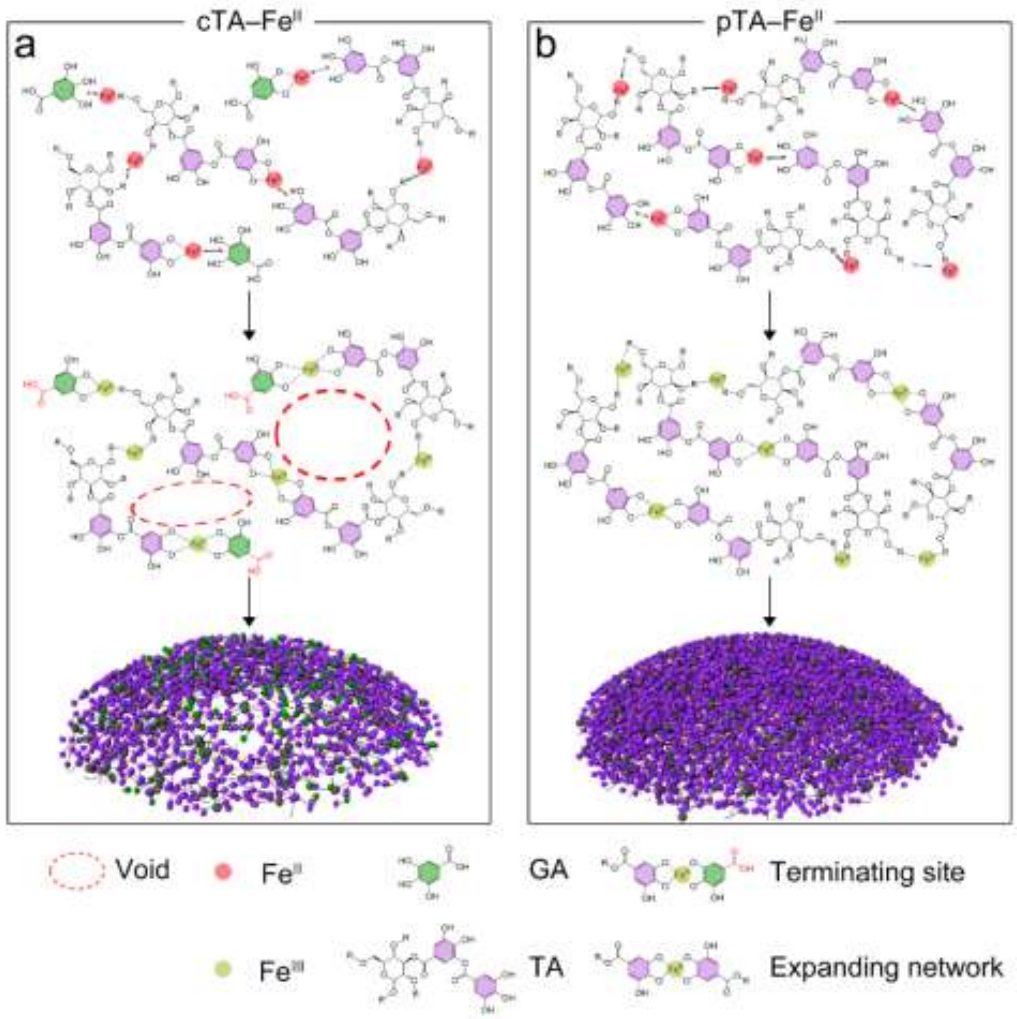
Figure 5. (a) Schematic representation of pore size and density of cTA–Fe^{II} (left) and pTA–Fe^{II} (right) MPNs on a PS substrate (blue). Each snapshot represents MPNs after saturated time. (b) Potential of mean force versus distance graphs of interactions between Fe^{II} ion in OA-based MPN cluster and free GA or TA. The interaction energies between MPNs and phenolic ligands were calculated under relative orientation. (c) Radial distribution function ($g(r)$) between Fe^{II} ions versus distance graphs in simulated cTA–Fe^{II} and pTA–Fe^{II} MPNs. (d) Density–time graphs of TA/GA phenolic mixtures with Fe^{II} ions. Each snapshot represents

This article is protected by copyright. All rights reserved.

Author Manuscript

16136829, 0, Downloaded from https://onlinelibrary.wiley.com/doi/10.1002/smll.202509224 by The University Of Melbourne, Wiley Online Library on [26/11/2025]. See the Terms and Conditions (https://onlinelibrary.wiley.com/terms-and-conditions) on Wiley Online Library for rules of use; OA articles are governed by the applicable Creative Commons License

MPNs after saturated time. (e) Density of MPNs formed with Fe^{II} or Fe^{III} and TA and GA mixtures at different ratios.



Scheme 2. (a) Schematic representation of the cTA–Fe^{II} network showing larger pores as GA terminating sites prevent network expansion. (b) Schematic representation of the pTA–Fe^{II} network without the terminating sites of GA, and hence forming a homogenous, less porous network.

3. Conclusion

We demonstrated the engineering of MPN properties by controlling, through refinement, the composition of the phenolic component used for the preparation of MPN films via OA. The selective purification of large polyphenol compounds from a broad range of phenolic molecules in commercially available TA afforded the assembly of denser and thicker MPN capsules as opposed to MPN capsules synthesized from a phenolic mixture. The differences between cTA–Fe^{II} and pTA–Fe^{II} were primarily attributed to the presence of low M_w phenolic ligands in cTA and the varying degrees of interactions between large multidentate

This article is protected by copyright. All rights reserved.

Author Manuscript

16136829, 0, Downloaded from https://onlinelibrary.wiley.com/doi/10.1002/smll.202509224 by The University Of Melbourne, Wiley Online Library on [26/11/2025]. See the Terms and Conditions (https://onlinelibrary.wiley.com/terms-and-conditions) on Wiley Online Library for rules of use; OA articles are governed by the applicable Creative Commons License

polyphenols, small phenolic ligands, and metal ions. MD simulations using a GA and TA mixture to simplistically model cTA further supported these findings.

In summary, the engineering of metal coordination complexes through phenolic compositional refinement enables tuning of thickness, stiffness, permeability, and mechanical properties of MPN films. Tunability of such properties can be used to rationally design MPN materials with properties that are tailored for their target application. For example, capsule thickness and permeability can be used to tune the release of encapsulated active molecules in drug delivery systems or control signal accessibility and sensitivity of sensing platforms. Adjustable film density and pore size can be used to regulate the selective transport of target gas species in gas separation membranes. Therefore, the results presented here demonstrate compositional refinement as a promising design strategy to bridge molecular-level engineering with application-specific performance in MPN materials.

Acknowledgements

This research was funded by the Australian Research Council (ARC) through the Discovery Project (DP240102343) Scheme. This work was performed in part at the Materials Characterisation and Fabrication Platform (MCFP), Biosciences Microscopy Unit, and the Bio21 Institute at The University of Melbourne. We acknowledge Dr. Francesca Cavalieri, Dr. Omid Mazaheri, and Dr. Wanjun Xu for their helpful discussions.

Received: ((will be filled in by the editorial staff))
Revised: ((will be filled in by the editorial staff))
Published online: ((will be filled in by the editorial staff))

References

[1] B. Qin, Z. Yin, X. Tang, S. Zhang, Y. Wu, J.-F. Xu, X. Zhang, "Supramolecular Polymer Chemistry: From Structural Control to Functional Assembly" *Prog. Polym. Sci.* **2020**, *100*, 101167.

[2] A. Legrand, L.-H. Liu, P. Royla, T. Aoyama, G. A. Craig, A. Carné-Sánchez, K. Urayama, J. J. Weigand, C.-H. Lin, S. Furukawa, "Spatiotemporal Control of Supramolecular Polymerization and Gelation of Metal–Organic Polyhedra" *J. Am. Chem. Soc.* **2021**, *143*, 3562–3570.

This article is protected by copyright. All rights reserved.

Author Manuscript

16136829, 0, Downloaded from https://onlinelibrary.wiley.com/doi/10.1002/smll.202509224 by The University Of Melbourne, Wiley Online Library on [26/11/2025]. See the Terms and Conditions (https://onlinelibrary.wiley.com/terms-and-conditions) on Wiley Online Library for rules of use; OA articles are governed by the applicable Creative Commons License

[3] Y. Qu, R. De Rose, C. Kim, J. Zhou, Z. Lin, Y. Ju, S. K. Bhangu, C. Cortez-Jugo, F. Cavalieri, F. Caruso, "Supramolecular Polyphenol-DNA Microparticles for In Vivo Adjuvant and Antigen Co-Delivery and Immune Stimulation" *Angew Chem. Int. Ed.* **2023**, *62*, e202214935.

[4] Y. Han, R. P. Lafleur, J. Zhou, W. Xu, Z. Lin, J. J. Richardson, F. Caruso, "Role of Molecular Interactions in Supramolecular Polypeptide–Polyphenol Networks for Engineering Functional Materials" *J. Am. Chem. Soc.* **2022**, *144*, 12510–12519.

[5] C.-J. Kim, F. Ercole, E. Goudeli, S. K. Bhangu, J. Chen, M. Faria, J. F. Quinn, F. Caruso, "Engineering Programmable DNA Particles and Capsules Using Catechol-Functionalized DNA Block Copolymers" *Chem. Mater.* **2022**, *34*, 7468–7480.

[6] Y. Han, J. Zhou, Y. Hu, Z. Lin, Y. Ma, J. J. Richardson, F. Caruso, "Polyphenol-Based Nanoparticles for Intracellular Protein Delivery Via Competing Supramolecular Interactions" *ACS Nano* **2020**, *14*, 12972–12981.

[7] C. Stoffelen, R. Munirathinam, W. Verboom, J. Huskens, "Self-assembly of Size-Tunable Supramolecular Nanoparticle Clusters in a Microfluidic Channel" *Mater. Horiz.* **2014**, *1*, 595–601.

[8] L. Bao, T. Xu, K. Guo, W. Huang, X. Lu, "Supramolecular Engineering of Crystalline Fullerene Micro-/Nano-Architectures" *Adv. Mater.* **2022**, *34*, 2200189.

[9] C. Kim, E. Goudeli, F. Ercole, Y. Ju, Y. Gu, W. Xu, J. F. Quinn, F. Caruso, "Particle Engineering Via Supramolecular Assembly of Macroscopic Hydrophobic Building Blocks" *Angew. Chem. Int. Ed.* **2024**, *63*, e202315297.

[10] M. Shin, J. H. Ryu, J. P. Park, K. Kim, J. W. Yang, H. Lee, "DNA/Tannic Acid Hybrid Gel Exhibiting Biodegradability, Extensibility, Tissue Adhesiveness, and Hemostatic Ability" *Adv. Funct. Mater.* **2015**, *25*, 1270–1278.

[11] H. Lin, L. Zhou, F. Mei, W. Dou, L. Hu, H. Yang, L. Xu, "Highly Efficient Self-Assembly of Metallacages and Their Supramolecular Catalysis Behaviors in Microdroplets" *Angew. Chem. Int. Ed.* **2023**, *62*, e202301900.

[12] H. Ejima, J. J. Richardson, K. Liang, J. P. Best, M. P. van Koeverden, G. K. Such, J. Cui, F. Caruso, "One-Step Assembly of Coordination Complexes for Versatile Film and Particle Engineering" *Science* **2013**, *341*, 154–157.

[13] J. Zhou, Z. Lin, Y. Ju, M. A. Rahim, J. J. Richardson, F. Caruso, "Polyphenol-Mediated Assembly for Particle Engineering" *Acc. Chem. Res.* **2020**, *53*, 1269–1278.

[14] H. Ejima, J. J. Richardson, F. Caruso, "Metal-Phenolic Networks as a Versatile Platform to Engineer Nanomaterials and Biointerfaces" *Nano Today* **2017**, *12*, 136–148.

Author Manuscript

This article is protected by copyright. All rights reserved.

16136829, 0, Downloaded from https://onlinelibrary.wiley.com/doi/10.1002/smll.202509224 by The University Of Melbourne, Wiley Online Library on [26/11/2025]. See the Terms and Conditions (https://onlinelibrary.wiley.com/terms-and-conditions) on Wiley Online Library for rules of use; OA articles are governed by the applicable Creative Commons License

[15] Z. Lin, J. Zhou, Y. Qu, S. Pan, Y. Han, R. P. Lafleur, J. Chen, C. Cortez-Jugo, J. J. Richardson, F. Caruso, "Luminescent Metal-Phenolic Networks for Multicolor Particle Labeling" *Angew. Chem., Int. Ed.* **2021**, *60*, 24968–24975.

[16] Y. Xu, Y. Guo, C. Zhang, M. Zhan, L. Jia, S. Song, C. Jiang, M. Shen, X. Shi, "Fibronectin-Coated Metal–Phenolic Networks for Cooperative Tumor Chemo-/Chemodynamic/Immune Therapy Via Enhanced Ferroptosis-Mediated Immunogenic Cell Death" *ACS Nano* **2022**, *16*, 984–996.

[17] Z. Lin, J. Zhou, C. Cortez-Jugo, Y. Han, Y. Ma, S. Pan, E. Hanssen, J. J. Richardson, F. Caruso, "Ordered Mesoporous Metal–Phenolic Network Particles" *J. Am. Chem. Soc.* **2020**, *142*, 335–341.

[18] M. A. Rahim, K. Kempe, M. Müllner, H. Ejima, Y. Ju, M. P. Van Koeverden, T. Suma, J. A. Braunger, M. G. Leeming, B. F. Abrahams, "Surface-Confined Amorphous Films from Metal-Coordinated Simple Phenolic Ligands" *Chem. Mater.* **2015**, *27*, 5825–5832.

[19] S. K. Bhangu, P. Charchar, B. B. Noble, C.-J. Kim, S. Pan, I. Yarovsky, F. Cavalieri, F. Caruso, "Origins of Structural Elasticity in Metal–Phenolic Networks Probed by Super-Resolution Microscopy and Multiscale Simulations" *ACS Nano* **2022**, *16*, 98–110.

[20] W. Xu, S. Pan, B. B. Noble, Z. Lin, S. Kaur Bhangu, C.-J. Kim, J. Chen, Y. Han, I. Yarovsky, F. Caruso, "Engineering Flexible Metal-Phenolic Networks with Guest Responsiveness via Intermolecular Interactions" *Angew. Chem. Int. Ed.* **2023**, *62*, e202302448.

[21] M. A. Rahim, M. Björnmalm, T. Suma, M. Faria, Y. Ju, K. Kempe, M. Müllner, H. Ejima, A. D. Stickland, F. Caruso, "Metal–Phenolic Supramolecular Gelation" *Angew. Chem. Int. Ed.* **2016**, *55*, 13803–13807.

[22] J. Chen, J. Li, J. Zhou, Z. Lin, F. Cavalieri, E. Czuba-Wojnilowicz, Y. Hu, A. Glab, Y. Ju, J. J. Richardson, "Metal–Phenolic Coatings as a Platform to Trigger Endosomal Escape of Nanoparticles" *ACS Nano* **2019**, *13*, 11653–11664.

[23] J. Guo, Y. Ping, H. Ejima, K. Alt, M. Meissner, J. J. Richardson, Y. Yan, K. Peter, D. Von Elverfeldt, C. E. Hagemeyer, "Engineering Multifunctional Capsules through the Assembly of Metal–Phenolic Networks" *Angew. Chem. Int. Ed.* **2014**, *53*, 5546–5551.

[24] Q.-Z. Zhong, S. Pan, Md. A. Rahim, G. Yun, J. Li, Y. Ju, Z. Lin, Y. Han, Y. Ma, J. J. Richardson, F. Caruso, "Spray Assembly of Metal–Phenolic Networks: Formation, Growth, and Applications" *ACS Appl. Mater. Interfaces* **2018**, *10*, 33721–33729.

This article is protected by copyright. All rights reserved.

Author Manuscript

16136829, 0, Downloaded from https://onlinelibrary.wiley.com/doi/10.1002/smll.202509224 by The University Of Melbourne, Wiley Online Library on [26/11/2025]. See the Terms and Conditions (https://onlinelibrary.wiley.com/terms-and-conditions) on Wiley Online Library for rules of use; OA articles are governed by the applicable Creative Commons License

[25] G. Yun, Q. A. Besford, S. T. Johnston, J. J. Richardson, S. Pan, M. Biviano, F. Caruso, "Self-Assembly of Nano- to Macroscopic Metal–Phenolic Materials" *Chem. Mater.* **2018**, *30*, 5750–5758.

[26] J. Chen, S. Pan, J. Zhou, Q.-Z. Zhong, Y. Qu, J. J. Richardson, F. Caruso, "Programmable Permeability of Metal–Phenolic Network Microcapsules" *Chem. Mater.* **2020**, *32*, 6975–6982.

[27] N. Li, Z. Shou, S. Yang, X. Cheng, C. Chen, S. Zheng, Y. Shi, H. Tang, "Subtle Distinction in Molecular Structure of Flavonoids Leads to Vastly Different Coating Efficiency and Mechanism of Metal-Polyphenol Networks with Excellent Antioxidant Activities" *Colloids Surf. B Biointerfaces* **2023**, *229*, 113454.

[28] M. A. Rahim, M. Björnmalm, N. Bertleff-Zieschang, Y. Ju, S. Mettu, M. G. Leeming, F. Caruso, "Multiligand Metal–Phenolic Assembly from Green Tea Infusions" *ACS Appl. Mater. Interfaces* **2018**, *10*, 7632–7639.

[29] G. Yun, J. J. Richardson, M. Biviano, F. Caruso, "Tuning the Mechanical Behavior of Metal–Phenolic Networks through Building Block Composition" *ACS Appl. Mater. Interfaces* **2019**, *11*, 6404–6410.

[30] G. Lin, M. A. Rahim, M. G. Leeming, C. Cortez-Jugo, Q. A. Besford, Y. Ju, Q.-Z. Zhong, S. T. Johnston, J. Zhou, F. Caruso, "Selective Metal–Phenolic Assembly from Complex Multicomponent Mixtures" *ACS Appl. Mater. Interfaces* **2019**, *11*, 17714–17721.

[31] P. Arapitsas, S. Menichetti, F. F. Vincieri, A. Romani, "Hydrolyzable Tannins with the Hexahydroxydiphenoyl Unit and the *m*-Depsidic Link: HPLC-DAD-MS Identification and Model Synthesis" *J. Agric. Food Chem.* **2007**, *55*, 48–55.

[32] H. P. Makkar, K. Becker, "Behaviour of Tannic Acid from Various Commercial Sources towards Redox, Metal Complexing and Protein Precipitation Assays of Tannins" *J. Sci. Food Agric.* **1993**, *62*, 295–299.

[33] G. Ghigo, S. Berto, M. Minella, D. Vione, E. Alladio, V. M. Nurchi, J. Lachowicz, P. G. Daniele, "New Insights into the Protogenic and Spectroscopic Properties of Commercial Tannic Acid: The Role of Gallic Acid Impurities" *New J. Chem.* **2018**, *42*, 7703–7712.

[34] H. Yuan, Q. Ma, L. Ye, G. Piao, "The Traditional Medicine and Modern Medicine from Natural Products" *Molecules* **2016**, *21*, 559.

[35] F. Maharani, I. Hartati, V. Paramita, "Review on Tannic Acid: Potensial Sources, Isolation Methods, Aplication and Bibliometric Analysis" *Res. Chem. Eng.* **2020**, *2*, 46–52.

This article is protected by copyright. All rights reserved.

Author Manuscript

16136829, 0, Downloaded from https://onlinelibrary.wiley.com/doi/10.1002/smll.202509224 by The University Of Melbourne, Wiley Online Library on [26/11/2025]. See the Terms and Conditions (https://onlinelibrary.wiley.com/terms-and-conditions) on Wiley Online Library for rules of use; OA articles are governed by the applicable Creative Commons License

[36] Q.-Z. Zhong, S. Li, J. Chen, K. Xie, S. Pan, J. J. Richardson, F. Caruso, "Oxidation-Mediated Kinetic Strategies for Engineering Metal–Phenolic Networks" *Angew. Chem. Int. Ed.* **2019**, *58*, 12563–12568.

[37] C.-E. Lin, M.-Y. Zhou, W.-S. Hung, B.-K. Zhu, K.-R. Lee, L.-P. Zhu, L.-F. Fang, "Ultrathin Nanofilm with Tailored Pore Size Fabricated by Metal-Phenolic Network for Precise and Rapid Molecular Separation" *Sep. Purif. Technol.* **2018**, *207*, 435–442.

[38] H. Lee, W. I. Kim, W. Youn, T. Park, S. Lee, T.-S. Kim, J. F. Mano, I. S. Choi, "Iron Gall Ink Revisited: In Situ Oxidation of Fe(II)–Tannin Complex for Fluidic-Interface Engineering" *Adv. Mater.* **2018**, *30*, 1805091.

[39] N. R. Perron, H. C. Wang, S. N. DeGuire, M. Jenkins, M. Lawson, J. L. Brumaghim, "Kinetics of Ironoxidation upon Polyphenol Binding" *Dalton Trans.* **2010**, *39*, 9982–9987.

[40] Y. Ju, C. Cortez-Jugo, J. Chen, T.-Y. Wang, A. J. Mitchell, E. Tsantikos, N. Bertleff-Zieschang, Y.-W. Lin, J. Song, Y. Cheng, "Engineering of Nebulized Metal–Phenolic Capsules for Controlled Pulmonary Deposition" *Adv. Sci.* **2020**, *7*, 1902650.

[41] C.-J. Kim, F. Ercole, Y. Ju, S. Pan, J. Chen, Y. Qu, J. F. Quinn, F. Caruso, "Synthesis of Customizable Macromolecular Conjugates as Building Blocks for Engineering Metal–Phenolic Network Capsules with Tailorable Properties" *Chem. Mater.* **2021**, *33*, 8477–8488.

[42] H. Sun, E. H. Wong, Y. Yan, J. Cui, Q. Dai, J. Guo, G. G. Qiao, F. Caruso, "The Role of Capsule Stiffness on Cellular Processing" *Chem. Sci.* **2015**, *6*, 3505–3514.

Supporting Information

Supporting Information is available from the Wiley Online Library or from the author.

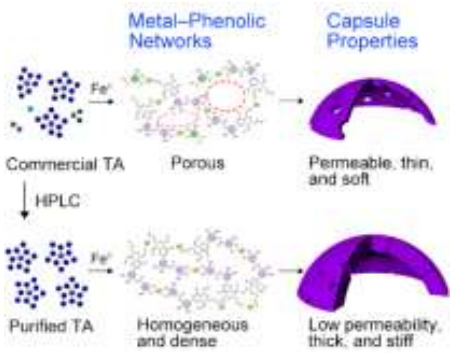
This article is protected by copyright. All rights reserved.

Author Manuscript

16136829, 0, Downloaded from https://onlinelibrary.wiley.com/doi/10.1002/smll.202509224 by The University Of Melbourne, Wiley Online Library on [26/11/2025]. See the Terms and Conditions (https://onlinelibrary.wiley.com/terms-and-conditions) on Wiley Online Library for rules of use; OA articles are governed by the applicable Creative Commons License

Purifying commercial tannic acid (TA) by high-performance liquid chromatography removes small phenolics so large species assemble into metal-phenolic networks (MPNs). This yields less permeable, thicker and stiffer MPN capsules than capsules prepared from commercial TA, thus demonstrating MPN engineering by compositional tuning of phenolic molecules.

Engineering Metal–Phenolic Network Materials through Compositional Tuning of Phenolic Molecules



Author Manuscript

This article is protected by copyright. All rights reserved.

16136829, 0, Downloaded from https://onlinelibrary.wiley.com/doi/10.1002/smll.202509224 by The University Of Melbourne, Wiley Online Library on [26/11/2025]. See the Terms and Conditions (https://onlinelibrary.wiley.com/terms-and-conditions) on Wiley Online Library for rules of use; OA articles are governed by the applicable Creative Commons License